OXFORD

ORIGINAL ARTICLE

YAP Is a Critical Inducer of SOCS3, Preventing Reactive Astrogliosis

Zhihui Huang[1,3,4], Ying Wang[1,3,5], Guoqing Hu[2], Jiliang Zhou[2], Lin Mei[1,3] and Wen-Cheng Xiong[1,3]

[1]Department of Neuroscience and Regenerative Medicine and Department of Neurology, [2]Department of Pharmacology and Toxicology, Medical College of Georgia, Georgia Regents University, Augusta, GA 30912, USA, [3]Charlie Norwood VA Medical Center, Augusta, GA 30912, USA, [4]Institute of Hypoxia Medicine and Institute of Neuroscience, Wenzhou Medical University, Wenzhou, Zhejiang 325035, China and [5]Research Center of Blood Transfusion Medicine, Key Laboratory of Laboratory Medicine (Wenzhou Medical University), Ministry of Education, Zhejiang Provincial People's Hospital, Hangzhou, Zhejiang 310014, China

Address correspondence to Wen-Cheng Xiong. Email: wxiong@gru.edu; Lin Mei. Email: lmei@gru.edu

Abstract

Yes-associated protein (YAP) is a key transcriptional cofactor of the Hippo pathway, critical for the development of multiple organs. However, its role in the developing brain remains poorly understood. Here, we found that YAP was highly expressed in astrocytes and YAP deletion elevated the astrocytic activation in culture and in vivo, which was associated with microglial activation. At the molecular level, YAP in astrocytes was activated by IFNβ or ciliary neurotrophic factor (CNTF), which was necessary for IFNβ or CNTF induction of the suppressor of cytokine signaling 3 (SOCS3), a negative regulator of the Janus kinase–signal transducer and activator of transcription (JAK–STAT) inflammatory pathway. YAP$^{-/-}$ astrocytes thus showed hyperactivation of the JAK–STAT inflammatory pathway and reactive astrogliosis. Expression of SOCS3 in YAP$^{-/-}$ astrocytes prevented the hyperactivation of STAT3 and partially restored the astrocytic activation. Finally, reactive astrogliosis was associated with blood–brain barrier dysfunction in YAP brain-selective knockout mice. Taken together, these results identify unrecognized functions of YAP in preventing reactive astrogliosis and reveal a pathway of YAP-SOCS for the negatively control of neuroinflammation.

Key words: blood–brain barrier, reactive astrogliosis, SOCS3, STAT3, YAP

Introduction

Astrocytes, a major type of glial cells in the brain, are crucial for a wide variety of functions in the central nervous system (CNS), including regulating synaptic neurotransmission (Eroglu and Barres 2010) and modulating blood flow (Takano et al. 2006). Under physiological condition, astrocytes give rise to a dense network of finely branching processes, some of which envelop blood vessel, and form blood–brain barrier (BBB) with endothelial cells and pericytes. BBB (neurovascular unit) is a physical and metabolic barrier between the CNS and the systemic circulation to maintain the microenvironment of the CNS (Abbott et al. 2010; Sofroniew and Vinters 2010; Liebner et al. 2011; Tajes et al. 2014). Recently, astrocytes are also considered to be a special type of immune neuroglia at the CNS (Farina et al. 2007; Ransohoff and Engelhardt 2012; Burda and Sofroniew 2014; Xie and Yang 2015). Under stress or pathological insults, astrocytes are

activated (so-called reactive astrogliosis) (Burda and Sofroniew 2014). The reactive astrocytes produce and release diverse pro- or anti-inflammatory cytokines, chemokines, and neutrophins to cause tissue damage or repair (Shen et al. 2012; Yang et al. 2012; Burda and Sofroniew 2014; Choi et al. 2014; Xie and Yang 2015). Although some signaling pathways, such as STAT3, are identified to regulate astrocyte activation (Burda and Sofroniew 2014), the molecular mechanisms of reactive astrogliosis under different pathological insults remain unclear.

The Hippo pathway is critical for the development of multiple organs, including liver, heart, kidney, and intestine (Pan 2010; Mo et al. 2014; Piccolo et al. 2014). Activation of this pathway leads to phosphorylation of Yes-associated protein (YAP), a transcriptional cofactor, and its subsequent proteosomal degradation or cytoplasmic retention. Dephosphorylated YAP enters nuclei and interacts with transcriptional enhancer factor domain family proteins to induce target gene expression. YAP is believed to control organ size by promoting cell proliferation, differentiation, and survival (Zhao et al. 2007; Pan 2010; Mo et al. 2014; Piccolo et al. 2014). A glaring gap in our understanding of YAP function is that little is known about its role in developing nervous system.

Here, we provide evidence that in developing brains, YAP was selectively expressed in astrocytes and neural stem cells (NSCs). YAP deletion resulted in reactive astrogliosis, astrocyte-driven microglial activation, which was associated with reduced BBB function. At the molecular level, YAP in astrocytes was necessary for preventing hyperactivation of the JAK/STAT inflammatory pathway, which was likely due to YAP induction of suppressor of cytokine signaling (SOCS) family gene expression. Taken together, these results reveal a pathway of YAP-SOCS for the negatively control of STAT-mediated inflammatory response and reactive astrogliosis, a crucial event for maintaining adequate BBB function.

Materials and Methods

Animals and Mouse Breeding

Yap^{nestin}-CKO conditional knockout mice were generated by crossing floxed Yap allele ($Yap^{f/f}$) with nestin-Cre transgenic mice. Both $Yap^{f/f}$ and nestin-Cre mice were maintained in C57BL/6 strain background. $Yap^{f/f}$ mice were generated as previously described (Zhang et al. 2010; Wang et al. 2014). Nestin-Cre transgenic mice were purchased from the Jackson Laboratory (donated by Dr Rudiger Klein). Briefly, we first generated nestin-Cre$^+$/YAP$^{f/w}$ mouse, by crossing nestin-Cre$^+$ male mice with $Yap^{f/f}$ female mice. Nestin-Cre$^+$/YAP$^{f/w}$ male mice were then breed with $Yap^{f/f}$ female mice. This breeding strategy yielded 25% progeny with the homozygous mice (Yap^{nestin}-CKO) and 25% $Yap^{f/f}$ as control littermates. Embryonic day (E) 0.5 was defined as noon of the day when the vaginal plug was detected. Identification of these mice was performed as described in Supplementary Figure 1. The use of experimental animals has been approved by the Institutional Animal Care and Use Committee (IACUC) at Georgia Regents University in accordance with the NIH guidelines.

Primary Cultures of Neural Stem Cells, Astrocytes, Microglia, and Neurons

For Yap^{nestin}-CKO neural stem cell culture, Nestin-Cre$^+$/YAP$^{f/w}$ male mice were used to breed with YAP$^{f/f}$ female mice. The pregnant mice (E14.5) were sacrificed, and embryonic mice were taken out. Genomic DNAs of each embryonic mouse were collected for genotyping, and littermates were used as controls. NSCs were prepared from embryonic mouse ganglionic eminence, following an established protocol (Wang and Yu 2013). Tissues dissected from mouse ganglionic eminence under a stereo microscope were dissociated by trituration 10–15 times gently with a 200-μL pipette tip to achieve single-cell suspension. The single-cell suspensions thus obtained were grown in Neurobasal-A medium (Life Technologies) supplemented with B$_{27}$ (Life Technologies), 2 mM L-glutamine (Life Technologies), basic fibroblast growth factor (bFGF, 20 ng/mL, Gibco), and EGF (20 ng/mL, Gibco). Neurospheres after 5–7 days were collected for passage or further analyses. In cases in which monolayer NSCs were needed for immunostaining, neurospheres at passage 2 or 3 were dissociated into single cells and seeded onto poly-L-ornithine and fibronectin-coated plates (sigma) to grow as monolayers. To avoid transformation, neurospheres were cultured within 1 month or for less than 5 passages.

Primary glial cultures, including astrocytes, microglia, and oligodendrocytes and oligodendrocyte precursor cells (OPCs), were prepared from the cerebral cortex of P1–P3 neonatal mice as described previously with slight modifications (Su et al. 2009). Briefly, cerebral cortex was removed, demembranated, chopped, and then incubated with 0.125% trypsin at 37 °C for 20 min. The cerebral cortex was dissociated into a single cell suspension by mechanical disruption. The cells were seeded on poly-L-lysine (PLL, 0.1 mg/mL, Sigma)-coated culture flasks and incubated in DMEM containing 10% fetal bovine serum (FBS, Gibco). After 6–8 days cultures, the cells become confluent. The loosely attached microglia were collected by shaking at 200 rpm for 1 h. The OPCs were removed from the monolayer cell culture by further shaking the cells overnight. Astrocytes were subsequently detached using 0.25% trypsin–EDTA (Life Technologies) and plated into PLL-coated 35 mm dishes or onto PLL-coated coverslips. The purity of GFAP$^+$ astrocytes and Iba1$^+$ microglia in our culture system is >95%. For IFNβ treatment (2 ng/mL, R&D) or CNTF (20 ng/mL, R&D), astrocytes were starved in DMEM without serum for one overnight before treatment. For astrocyte transfection, we used rat Astrocyte Nucleofector Kit (Amaxa, Cologne, Germany) according to the manufacturer's instructions (program T-20). The Flag-SOCS3 plasmid was purchased from Addgene (donated by Dr Ronald Kahn), co-transfected with GFP (ratio, 3 : 1).

Dissociated cortical neurons were cultured as follows. Briefly, cortical tissues were isolated from E16 mouse embryos, and then were digested with 0.125% trypsin for 20 min at 37°C, followed by trituration with pipettes in the plating medium (DMEM with 10% FBS). Dissociated neurons were plated onto coverslips or 35 mm dishes coated with PLL (100 μg/mL; Sigma). After culturing for 6 h, media were changed into neuronal culture media (Neurobasal medium supplemented with 1% glutamate and 2% B27; Invitrogen). The culture medium was replaced every 3 days.

Western Blot and Nuclear Coimmunoprecipitation

Brain tissues or cultured cells were lysed in the lysis buffer [50 mM Tris–HCl (pH 7.4), 150 mM NaCl, 1% NP-40, 0.5% Triton X-100, 1 mM phenylmethylsulfonyl fluoride, 1 mM EDTA, 5 mM sodium fluoride, 2 mM sodium orthovanadate, and protease inhibitor cocktail] for 30 min on ice and centrifuged at 14 000 g for 20 min, and protein concentration was determined by the BCA protein assay kit (Thermo). Proteins were separated by 8–12% SDS–PAGE gel electrophoresis and transferred onto the nitrocellulose membrane. Blotted membranes were blocked in 10% skim milk at room temperature for 1 h and incubated with primary antibody overnight at 4 °C, rinsed and incubated for 1 h at room temperature with an appropriate horseradish peroxidase-conjugated secondary antibody (1 : 5000, Thermo). Chemiluminescent detection was performed with the ECL kit (Pierce, Rockford,

IL, USA). Primary antibodies included mouse monoclonal anti-YAP (1 : 1000, Sigma), anti-GFAP (1 : 1000, Millipore), anti-nestin (1 : 1000, Sigma), or rabbit polyclonal anti-p-YAP-Ser127 (1 : 1000, CST); p-STAT1-Tyr701 (1 : 1000, CST); p-STAT3-Tyr705 (1 : 1000, CST), STAT3 (1 : 1000, CST), p-JNK-T183/Y185 (1 : 1000, CST), JNK (1 : 1000, CST), p-p38-T180/Y182 (1 : 1000, CST), p-38 (1 : 1000, CST), p-IκBα-Ser32 (1 : 1000, CST), p-Akt-Ser473 (1 : 1000, CST), Akt (1 : 1000, CST), SOCS1 (1 : 1000, CST), SOCS3 (1 : 1000, CST). β-Actin or GAPDH as a loading control was detected alongside the experimental samples (1 : 3000, Sigma). For semi-quantitative analysis, protein bands detected by ECL were scanned into pictures and analyzed using the Image J software (National Institutes of Health).

For coimmunoprecipitation of STAT3 and YAP, primary cultured astrocytes were starved with DMEM without serum media for one overnight before IFNβ treatment. Primary cultured astrocytes after IFNβ treatment (2 ng/mL), nuclear protein was harvested for coimmnoprecipitation assays with an anti-STAT3 antibody (1 : 100, CST) by using the Nuclear Complex Co-IP kit (Active Motif). Western blot was performed using an YAP antibody as described above.

Quantitative Real-Time PCR Analysis

For real-time (RT)-PCR, total RNA was extracted from cultures of purified astrocytes with Trizol reagent (Invitrogen), converted to cDNA using the Revert AidFirst Strand cDNA Synthesis Kit (Thermo). PCR array was performed to screen cytokine- and chemokine-related gene expression profile using the Inflammatory Cytokines and Receptors PCR Array kit (SABiosciences, mouse) as described in the previous studies (Wang et al. 2014). cDNA products were amplified in 20 μL of reaction mixture containing the SYBR GreenER™ qPCR SuperMix Universal (Invitrogen) with respective gene-specific primers as previously reported otherwise were listed in Supplementary Table 1. Each amplification cycle consisted of an initial step at 95°C (5 min), followed by 40 cycles of denaturation at 95°C (15 s), annealing at 60°C (1 min). All samples were amplified in duplicate and every experiment was repeated at least independently 2 times. Relative gene expression was converted using the $2^{-\Delta\Delta C_t}$ method against the internal control, hypoxanthine phosphoribosyltransferase 1.

Immunostaining

For brain tissue section staining, brains of P0–P1 mice were directly removed and fixed in fresh 4% paraformaldehyde (PFA) for 2 days, and older mice brains were removed and fixed in 4% PFA for 2 days after transcardial perfusion. Then brains were dehydrated in 15%, 30% sucrose in PBS for 1–2 days, and cryopreserved in OCT compound for brain section. Longitudinal or coronal sections of 20–30 μm were cut on a freezing microtome and immediately processed for immunostaining of 1 h blocking in 10% BSA plus 0.3% Triton X-100 at room temperature, overnight incubation with primary antibodies at 4 °C, and for 1 h at room temperature incubation with appropriate secondary antibodies (1 : 1000, Molecular Probes, Eugene, OR, USA). For cultured cells staining, cells fixed with fresh 4% PFA in 0.1 M PBS (pH 7.4) for 20 min. After washing with PBS, cells were permeabilized with 0.1% Triton X-100 in 0.1 M PBS for 5 min, followed by incubation in blocking buffer (5% BSA and 0.1% Triton X-100 in 0.1 M PBS, pH 7.4) for 1 h, and incubated overnight at 4 °C with primary antibodies diluted in the blocking buffer. Cells were washed 3 times with PBS and incubated for 1 h at room temperature with an appropriate fluorescence-conjugated secondary antibody (1 : 1000, Molecular probes). The primary antibodies were rabbit polyclonal antibodies against Nestin (1 : 200, Sigma), anti-BLBP (1 : 300, Abcam), anti-p-STAT3-Tyr705 (1 : 200, CST), anti-

Flag (1 : 1000, CST), anti-GFAP (1 : 500, Millipore), anti-CD68 (1 : 200, Abcam), anti-Oligo-2 (1 : 500, Millipore), anti-Ki67 (1 : 200, Millipore), anti-PH3 (1 : 200, Millipore), anti-laminin (1 : 500, Abcam), or with a monoclonal antibodies against YAP (1 : 200, Sigma), anti-GFAP (1 : 500, Millipore), anti-Nestin (1 : 500, Millipore), anti-MAP-2 (1 : 500, Millipore), or with goat polyclonal antibodies against Iba1(1 : 500, Abcam) and doublecortin (1 : 200, Santa Cruz). Sections or cells were stained for DAPI (1 : 1000, Molecular Probes) to visualize nucleus. For visualization of F-actin, cells were incubated with rhodamine-conjugated phalloidin (1 : 60, Molecular Probes) at room temperature for 1 h. No positive signal was observed in control incubations using no primary antibody. Images were acquired on a Zeiss confocal system (FM300) using a multitrack configuration and processed using the Zeiss confocal software and the Adobe Photoshop CS 8.0 software.

Intravenous Injection of Tracers and Their Detection

Tracer injection was as described previously with slight modifications (Armulik et al. 2010). Briefly, tracers were injected intravenously into the tail vein in P20–P25 mice. The following tracers were used: Evans Blue (EB; 2% in PBS, 80 μL/20 g, Sigma Aldrich) and lysine-fixable 70 kDa dextran conjugated to tetramethylrhodamine (25 mg/mL in saline, 2 mg/20 g, Invitrogen). Images of dissected brains were captured by a stereomicroscope equipped with HBO 100 lamp (Carl Zeiss). EB in the brain was quantified by spectrophotometry as described previously (Armulik et al. 2010). For in situ detection of fluorophore-conjugated tracers, anaesthetized animals were perfused for 1–2 min with PBS, followed by 5 min perfusion with 4% PFA in PBS, pH 7.2. Brains were removed and the tissue was post-fixed in 4% PFA in PBS, pH 7.2, at 4 °C for overnight. Then brains were dehydrated in 30% sucrose in PBS for 1–2 days and cryopreserved in OCT compound for brain section. Longitudinal brain sections of 30 μm were cut on a freezing microtome and were immunostained with an anti-laminin (1 : 500, Abcam) antibody. Images were acquired on a Zeiss confocal system (FM300) using a multitrack configuration and processed using the Zeiss confocal software and the Adobe Photoshop CS 8.0 software.

Electron Microscope

YAP[f/f] and Yap[nestin]-CKO mice at P20 were perfused with fixative [4% PFA, 2% glutaraldehyde in 0.1 M sodium cacodylate (NaCac) buffer, pH 7.4] and left to sit for 1 h before brain was removed. Fixed brains were vibratomed at 100 μm thickness. And, cortex area for BBB analysis was dissected, agar embedded, post-fixed in 2% osmium tetroxide in NaCac, stained en bloc with 2% uranyl acetate, dehydrated with a graded ethanol series, and embedded in Epon–Araldite resin. Thin sections were cut with a diamond knife on an Leica EM UC6 ultramicrotome (Leica Microsystems, Inc., Bannockburn, IL, USA), collected on copper grids, and stained with uranyl acetate and lead citrate. Cells were observed in a JEM 1230 transmission electron microscope (JEOL USA, Inc., Peabody, MA, USA) at 110 kV and imaged with an UltraScan 4000 CCD camera and a First Light Digital Camera Controller (Gatan, Inc., Pleasanton, CA, USA). The astrocyte areas of surrounding blood vessels were analyzed by investigators unaware of genotypes using Image J.

Statistical Analysis

All data presented represent results from at least 3 independent experiments. Statistical analysis was performed using Student's t-test, or using an ANOVA with pair-wise comparisons. Statistical significance was defined as $P < 0.05$.

Results

YAP Expression in Astrocytes and NSCs

To understand the potential function of YAP in brain, we first examined its expression in the mouse brain. The YAP antibodies we used for immunohistochemical staining analysis of mouse brain sections appeared to be nonspecific. We thus examined YAP distribution in primary cultured brain cells, focusing on nestin[+] NSCs as well as their derivatives including neurons, astrocytes, and oligodendrocytes (Moyse et al. 2008). Coimmunostaining analysis using antibodies against YAP and cell type-specific markers showed that YAP was detected in most nestin[+] NSCs (Fig. 1A, G) and GFAP[+] astrocytes (Fig. 1B,G), but not in MAP2^{+} cortical neurons (Fig. 1C,G) or Oligo2^{+} oligodendrocytes (Fig. 1D,G). YAP was undetectable in doublecortin^{+} immature neurons (Fig. 1E,G) or Iba1^{+} microglia (Fig. 1F,G). The selective expression of YAP in NSCs and astrocytes was further confirmed by western blot analyses (Fig. 1H,I). It is of interest to note that the YAP protein was mainly distributed in the cytoplasm of NSCs, but in the nuclei of astrocytes under normal cultured condition (Fig. 1A,B,J). The YAP antibody was specific, as its immunosignal by both immunostaining and western blot analyses was abolished in YAP-deleted NSCs and astrocytes (Fig. 1A,B,I). These results demonstrate a selective expression of YAP in astrocytes and NSCs.

Reduced Astrocytic Proliferation Accompanied with Elevated Astrocytic Activation in YAP^{−/−} Astrocytes in Culture and In Vivo

The nuclear YAP is a main active form of YAP, which is critical for cell proliferation (Pan 2010; Mo et al. 2014; Piccolo et al. 2014). The nuclear distribution of YAP in astrocytes, but not in NSCs, thus led to the speculation for a critical role of YAP in regulating astrocyte proliferation. As expected, marked reductions in Ki67^{+} and PH3^{+} (both markers for cell proliferation) astrocytes were detected in Yap^{−/−} culture, compared with that of controls (Supplementary Fig. 2A–D), indicating a necessity of YAP for astrocytic proliferation in culture. Unexpectedly, both nestin and GFAP, markers of reactive astrocytes (Pekny et al. 2014), were higher in YAP^{−/−} astrocytes than that of controls by both immunostaining and western blot analyses (Fig. 2A–D), suggesting a necessity of YAP to prevent astrocytic activation in culture. This view was further supported by RT-PCR analysis of the transcripts of nestin and GFAP, and both transcripts were increased in YAP^{−/−} astrocytes (Fig. 2E). Taken together, these results suggest that while YAP in astrocytes is required for cell proliferation, it may also play a role in preventing astrocytic activation.

We further tested YAP's function in promoting astrocytic proliferation and suppressing astrocytic activation in vivo. Brain lipid-binding protein (BLBP) is a marker for radial glia and
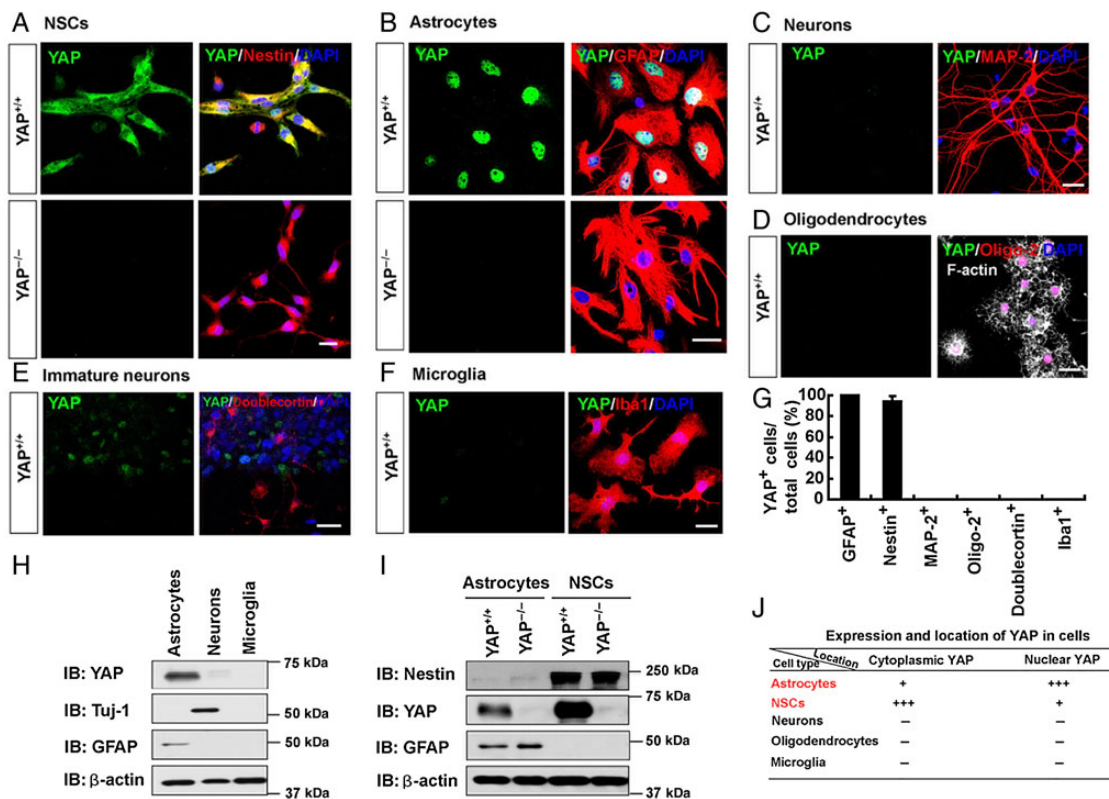

Figure 1. Selective expressions of YAP in cortical astrocytes and NSCs. (A–F) Double immunostaining of YAP (green) and nestin (red) in primary cultured WT and YAP^{−/−} cortical NSCs (A), and YAP (green) and GFAP (red) in primary cultured WT and YAP^{−/−} cortical astrocytes (B); YAP (green) and MAP-2 (red) in primary cultured cortical neurons (DIV 7) (C), YAP (green) and oligo-2 (red) in primary cultured oligodendrocytes (D), YAP (green) and doublecortin (red) in neurons (DIV 1) differentiated from NSCs (E), and YAP (green) and Iba1 (red) in primary cultured microglia (F) from WT mice. DAPI (blue) was used to stain cellular nuclei and F-actin (white) in (D) to stain the morphology of oligodendrocytes. Scale bars, 20 μm. (G) Quantitative analysis showing the percentages of YAP-positive cells over total cultured cells in one field (n = 10 for astrocytes and NSCs, n = 8 for mature neurons and oligodendrocytes, and n = 5 for microglia and immature neurons). (H and I) Western blot analysis of YAP expression in primary cultured WT astrocytes, neurons, microglia (H), and in cultured WT and YAP^{−/−} astrocytes and NSCs (I). (J) Summary table showed the expression and subcellular location of YAP in the cortical cells. Data were mean ± SD.
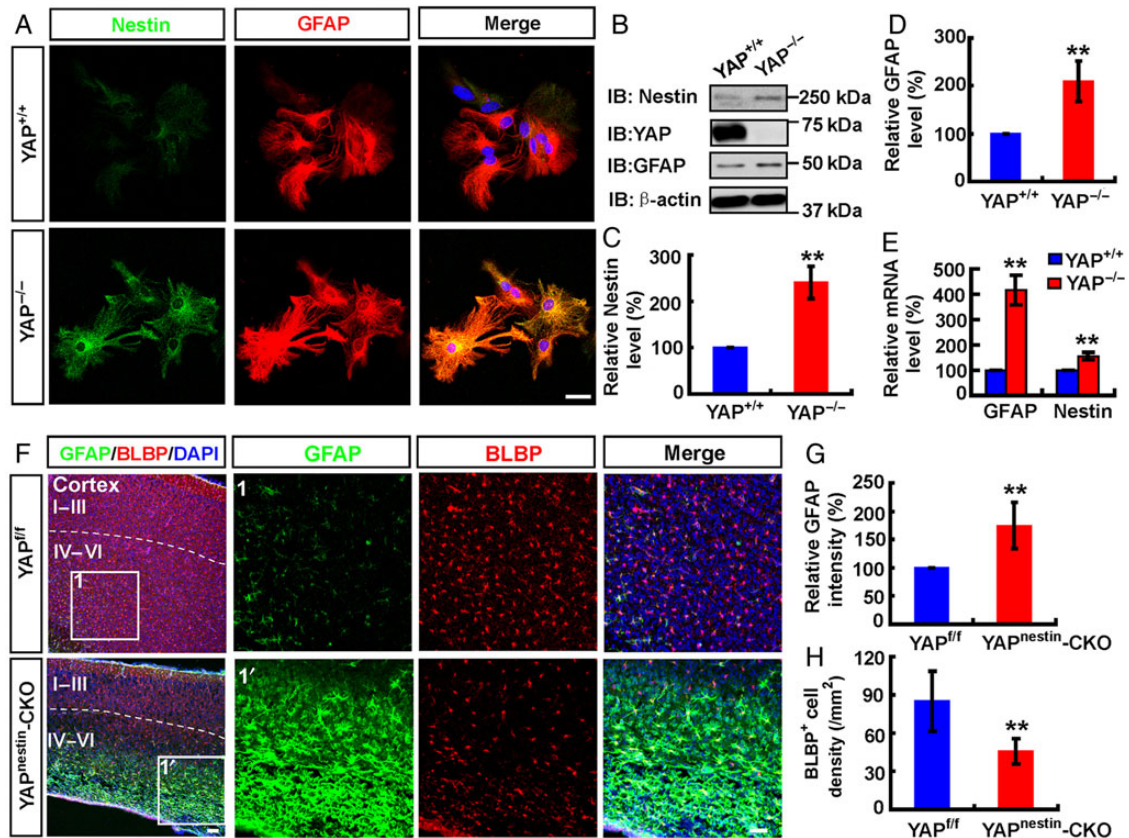
Figure 2. Elevated reactive astrocytes in Yap[nestin]-CKO cortex. (A) Double immunostaining analysis of Nestin (green) and GFAP (red) in cultured WT and YAP^{−/−} astrocytes. (B) Western blot analysis of Nestin and GFAP level in cultured WT and YAP^{−/−} astrocytes. (C and D) Quantitative analysis of Nestin (C) and GFAP (D) protein level as shown in (B) ($n = 3$ per group, normalized to WT). (E) RT-PCR analysis showed the relative gene expression of GFAP and Nestin in WT and YAP^{−/−} astrocytes. (F) Double immunostaining analysis of GFAP (green) and BLBP (red) in P7 cortex of Yap[f/f] and Yap[nestin]-CKO mice (sagittal sections). Selected regions 1 and 1′ were shown at higher magnification. (G and H) Quantitative analysis of the GFAP intensity (G) and BLBP-positive cell density (H) as shown in (F) ($n = 6$ per group). Scale bars, 20 μm. Data were mean ± SD. **$P < 0.01$, compared with the control group, Student's t-test.

neonatal cortical astrocytes (Guo et al. 2009; Ge et al. 2012). Interestingly, whereas the BLBP^{+} cells were reduced, GFAP^{+} cells were markedly increased, in Yap[nestin]-CKO cortex, particularly in the layers VI–VI, compared with their littermate controls (Fig. 2F,G, H). The GFAP[+] astrocytes' morphology appeared to be "activated" (Fig. 2F). These results are in line with the studies in culture, suggesting that YAP in astrocytes not only promotes cell proliferation, but also suppresses the astrocytic activation.

Astrocyte-Driven Microglial Activation in Yap[nestin]-CKO Cortex

Astrocyte activation often causes microglial activation (Burda and Sofroniew 2014). We thus tested this view by examining Iba1^{+} microglia in Yap[nestin]-CKO cortex. Indeed, as shown in Figure 3A–C, a large number of Iba1^{+} microglia or macrophages were detected in the mutant cortex, which was accompanied with the increased GFAP[+] astrocytes as well as the laminin-labeled blood vessels. These Iba1^{+} cells appeared in round or amoeboid-like morphology (Fig. 3A). The GFAP[+] astrocytes and microglia were barely increased in P3 mutant cortex, and more dramatically increased in P7 or older (e.g., P20) mutant brain, compared with their littermate controls (Fig. 3D,E). Taken together, these results revealed an age-dependent and temporally associated astrocytic-microglial "activation" in Yap mutant brain.

The temporal association of reactive astrogliosis with the microglial activation, and the selective YAP expression in

astrocytes, but not in microglia/macrophages, lead to a speculation that the reactive astrocytes in YAP mutant cortex may cause microglial activation. To test this view, primary microglia derived from wild-type (WT) cortex were incubated with the conditional media (CM) from WT (WT-CM) and Yap^{−/−} astrocytes (mutant CM) for overnight. As shown in Figure 3F, the microglial morphology was altered after exposure to CM from Yap^{−/−} astrocytes. While approximately 20% of microglia exposed to WT-CM showed membrane ruffling, a majority (82.3 ± 12.1%) of microglia exhibited membrane ruffling after exposed to the mutant CM (Fig. 3F,G). Both CD68 and Iba1 were increased in microglia exposed to the mutant CM, compared with that of WT-CM (Fig. 3F,H). Western blot results also showed an increased p-STAT3 (an inflammatory signaling marker) in microglia exposed to the mutant CM, compared with that of WT-CM (Fig. 3I,J). Taken together, these results suggest that microglia were activated likely by some factors secreted from YAP-deleted astrocytes.

Increased Expression of Inflammatory Factors and Hyperactivation of JAK–STAT Pathways in YAP^{−/−} Astrocytes

To further understand how YAP^{−/−} astrocytes activate microglia, we employed polymerase chain reaction-based array (PCR array) to analyze the expression of cytokine/chemokine-related genes in YAP^{−/−} astrocytes and WT controls (Supplementary Fig. 3A,B).
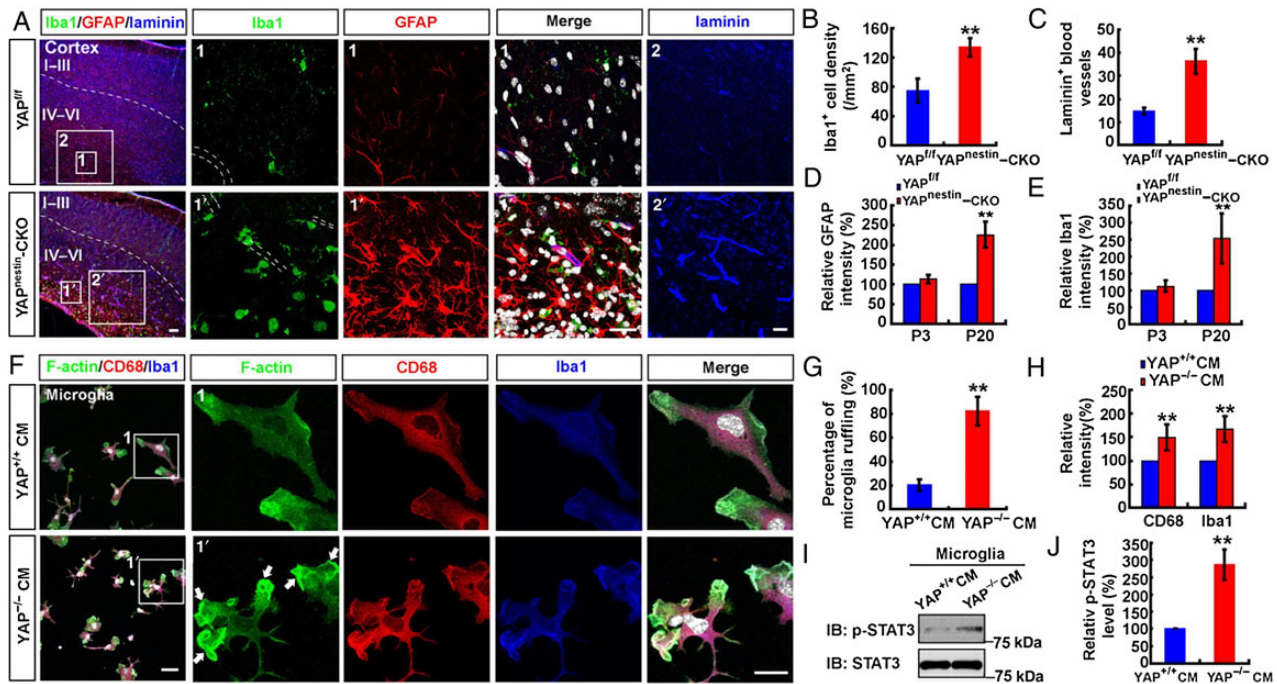
Figure 3. Astrocytes-driven microglia activation in Yap[nestin]-CKO cortex. (A) Triple immunostaining analysis of Iba1 (green), GFAP (red), and laminin (blue) in P7 cortex of Yap[f/f] and Yap[nestin]-CKO mice (sagittal sections). Selected regions 1, 2 and 1′, 2′ were shown at higher magnification. White dotted lines highlight the blood vessels. (B and C) Quantitative analysis of Iba1-positive cell density (B) and the number of laminin-positive blood vessels (C) in P7 cortex of Yap[f/f] and Yap[nestin]-CKO mice (n = 8 per group) as shown in (A). (D and E) Quantitative analysis of GFAP (D) and Iba1 intensity (E) at P3 and P20 cortex of Yap[f/f] and Yap[nestin]-CKO mice (n = 6 per group, normalized to WT). (F) Triple immunostaining analysis of F-actin (green), CD68 (red, a microglia activation marker), and Iba1 (blue, marker of microglia) in cultured WT microglia incubated with CM from cultured WT or YAP^{−/−} astrocytes (mutant). The selected regions 1 and 1′ were shown at higher magnification. White arrows indicated membrane ruffle of microglia. (G and H) Quantification of the percentages of microglia ruffling (G) (n = 8 per group), CD68 and Iba1 (H) intensity in microglia (n = 50 per group, normalized to the WT group) as shown in (F). (I) Western blot detected the expression level of p-STAT3 and STAT3 in WT microglia incubated with WT astrocyte CM or YAP^{−/−} astrocyte CM. (J) Quantitative analysis of western blot data as shown in (I) (n = 3 per group, normalized to WT). Scale bars, 20 μm. Data were mean ± SD. **P < 0.01, compared with the control group, Student's t-test.

Remarkably, >50% of the tested genes (35/62) were significantly increased in YAP^{−/−} astrocytes (fold >1.5), which include members of chemokine, interleukin, cytokine, and TNF families (Supplementary Fig. 3A,B and Fig. 4A). Among 35 increased genes, there were 17 in chemokine family, 6 in interleukin family, 4 in TNF family, and 8 other cytokines (Fig. 4A–C). Among 12 decreased genes, there were 2 in chemokine family, 6 in interleukin family, 2 in TNF family, and 2 other cytokines (Fig. 4A–C). RT-PCR analysis of some of these genes, such as Ccl3, Ccl9, TNF-α, and IL4, reconfirmed this view (Fig. 4D). In addition, we also detected increased expression of VEGF and TGFβ1 in YAP^{−/−} astrocytes (Fig. 4D).

The elevated cytokines/chemokines in YAP^{−/−} astrocytes may activate inflammatory signaling pathways in both astrocytes and microglia, which further increase the expression of inflammatory factors, forming a vicious cycle. Indeed, the inflammation-related signaling pathways, such as phospho-STAT3 (p-STAT3), phospho-JNK (p-JNK), and phospho-IκBα (p-IκBα), were all elevated in YAP^{−/−} astrocytes, whereas the levels of phospho-p38 (p-P38) and phospho-Akt (p-AKT) were comparable to that of controls (Fig. 4E,F). These results provide additional evidence for hyperactivation of inflammatory pathways in YAP-deficient astrocytes, which may cause microglial activation and increased angiogenesis.

YAP Induction of SOCS: a Crucial Family of Proteins That Negatively Regulate JAK–STAT Inflammatory Response

How does YAP in astrocytes suppress multiple cytokine/chemokine expression? YAP is believed to be a transcriptional activator

(Mo et al. 2014; Piccolo et al. 2014); thus, it is unlikely for YAP to directly suppress the expression of these cytokine/chemokine genes. Note that the SOCS family proteins play a crucial role in the negative control of cytokine-induced signaling and cytokine expression, preventing the vicious cycle (Yoshimura et al. 2007). We thus examined SOCS family protein expression in WT and YAP^{−/−} astrocytes. SOCS1, 2, and 3 were focused, because they were more abundantly expressed than other SOCSs (SOCS4, 5, 6, and 7; Supplementary Fig. 3C) and are well studied in astrocytes (Qin et al. 2008). Remarkably, SOCS1, 2, and 3 were all lower in YAP^{−/−} astrocytes than that of WT controls (Fig. 4G,H), suggesting a role for YAP to induce SOCS1–3 expression.

IFNβ is known to induce SOCS1/3 expression in primary astrocytes (Qin et al. 2008). We thus first tested whether YAP contributes to this pathway. Primary WT astrocytes were treated by IFNβ. As shown in Figure 5A, B, whereas p-STAT1 and p-STAT3 were induced by IFNβ, both YAP protein and phospho-YAP (ser127) were increased in a time-dependent manner, in line with a recent report for increased YAP in gp130 overexpressing epithelial cells (Taniguchi et al. 2015), providing a support for YAP to be involved in the IFNβ pathway. However, the increased YAP was not due to an increase at the transcriptional level, as no change in the mRNA level of YAP was detected in astrocytes treated with IFNβ (Fig. 5C). We then examined whether IFNβ "activates" YAP by promoting YAP nuclear localization. Indeed, double immunostaining analysis showed an increased nuclear translocation of YAP in GFAP^{+} cells stimulated by IFNβ (Fig. 5D,E), where YAP was colocalized with p-STAT3 (Fig. 5F). We further
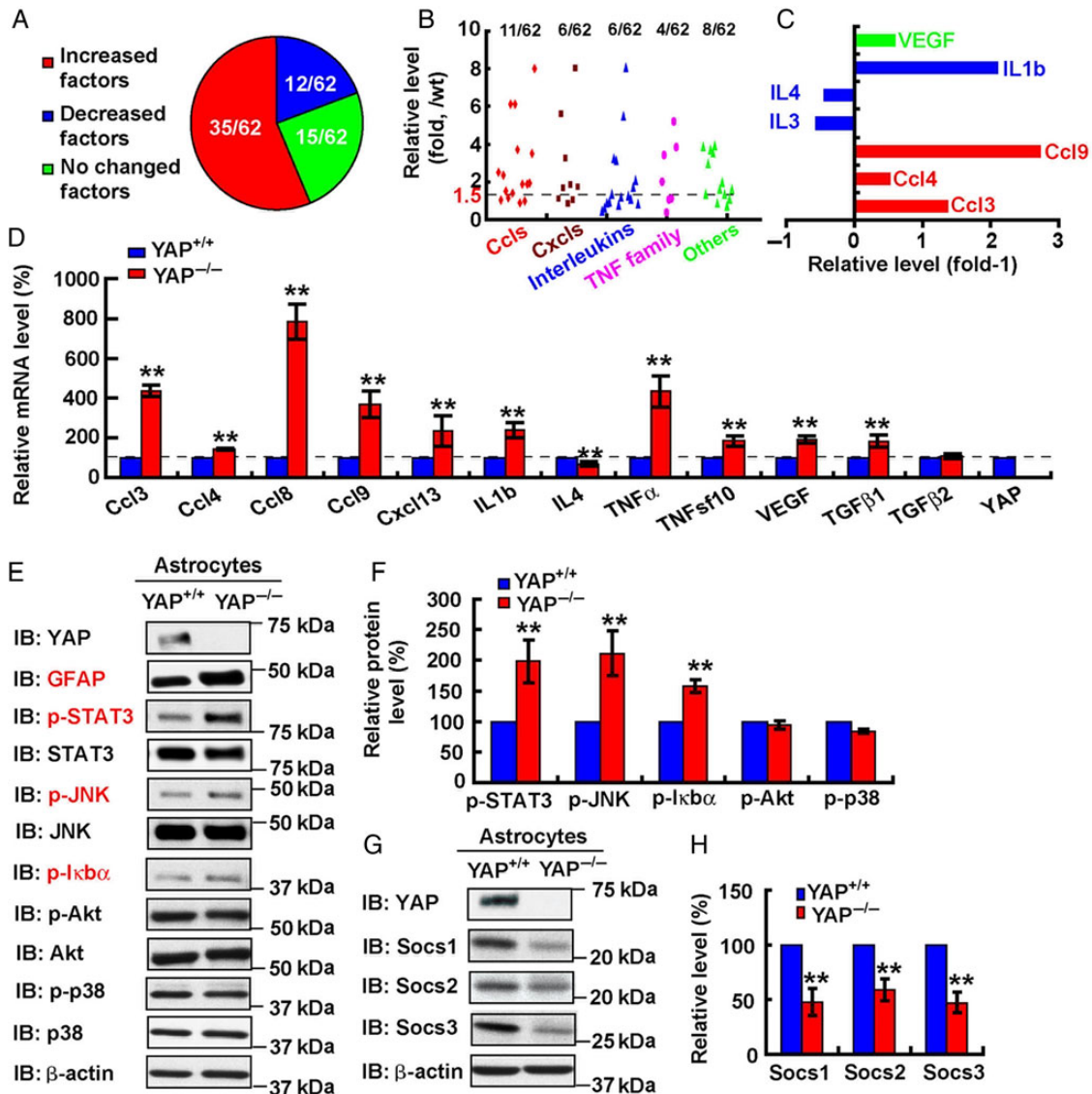
Figure 4. The altered expression of cytokines/chemokines and inflammation reaction in YAP$^{-/-}$ astrocytes. (A) Analysis of the altered factor genes in YAP$^{-/-}$ astrocytes by PCR array assays, compared with WT astrocytes. (B) Scatter diagram showed the change fold of cytokine/chemokine subfamilies (compared with WT control) in YAP$^{-/-}$ astrocytes by PCR array assays. (C) Samples of altered genes in YAP$^{-/-}$ astrocytes. (D) RT-PCR analysis showed the relative gene expression level in cultured WT and YAP$^{-/-}$ astrocytes ($n = 4$ per group, normalized to WT). (E) Western blot detected the inflammation-related signaling pathways in WT and YAP$^{-/-}$ astrocytes. (F) Quantitative analysis of western blot data as shown in (E) ($n = 3$ per group, normalized to WT). (G) Western blot detected the expression level of SOCS1, SOCS2, and SOCS3 in WT and YAP$^{-/-}$ astrocytes. (H) Quantitative analysis of western blot data as shown in (G) ($n = 3$ per group, normalized to WT). Data were mean ± SEM. **$P < 0.01$, compared with the control group, Student's t-test.

tested if the nuclear YAP forms a complex with p-STAT3 by coimmunoprecipitation experiments. As expected, YAP was detected in the STAT3 immunocomplex, which was stimulated by IFNβ (Fig. 5G). Taken together, these results suggest that YAP is "activated" by IFNβ, and once activated, the nuclear YAP interacts with the p-STAT3.

Is YAP required for IFNβ signaling pathway as well as the induction of SOCS1/3 expression? To address this question, primary WT and YAP$^{-/-}$ astrocytes were treated by IFNβ, and IFNβ-induced signaling (e.g., p-STAT3) was examined. As shown in Figure 6A,B, both the p-STAT1 and p-STAT3 levels were induced in both WT and YAP$^{-/-}$ astrocytes exposed to IFNβ. However, SOCS1 and SOCS3 were only induced in WT astrocytes as reported (Qin et al. 2008), but little to no induction of SOCS1/3 was detected in YAP$^{-/-}$ astrocytes in response to IFNβ (Fig. 6A,C,D).

In quantifying the p-STAT3 level, a more dramatic increase was detected in IFNβ-stimulated YAP$^{-/-}$ astrocytes, compared with that of WT controls (Fig. 6A,B), supporting the view for an impairment in SOCS-mediated negative feedback control of JAK–STAT pathway in YAP$^{-/-}$ astrocytes. We next examined IFNβ-induced transcriptional expression of SOCS3 and chemokines in WT and YAP$^{-/-}$ astrocytes by RT-PCR analysis. Consistently, IFNβ-induced transcriptional expression of SOCS3 was abolished in YAP$^{-/-}$ astrocytes (Fig. 6E). However, the induction of chemokines, such as CCL3, CCL4, and CCL8, was even more dramatic in YAP$^{-/-}$ astrocytes, compared with that of WT controls (Fig. 6E). We further examined if YAP is also regulated by CNTF, another ligand of JAK–STAT inflammatory pathway. Indeed, as IFNβ, CNTF induced a more dramatic increase of p-STAT3 in YAP$^{-/-}$ cells than in WT cells (Supplementary Fig. 4A,B), and
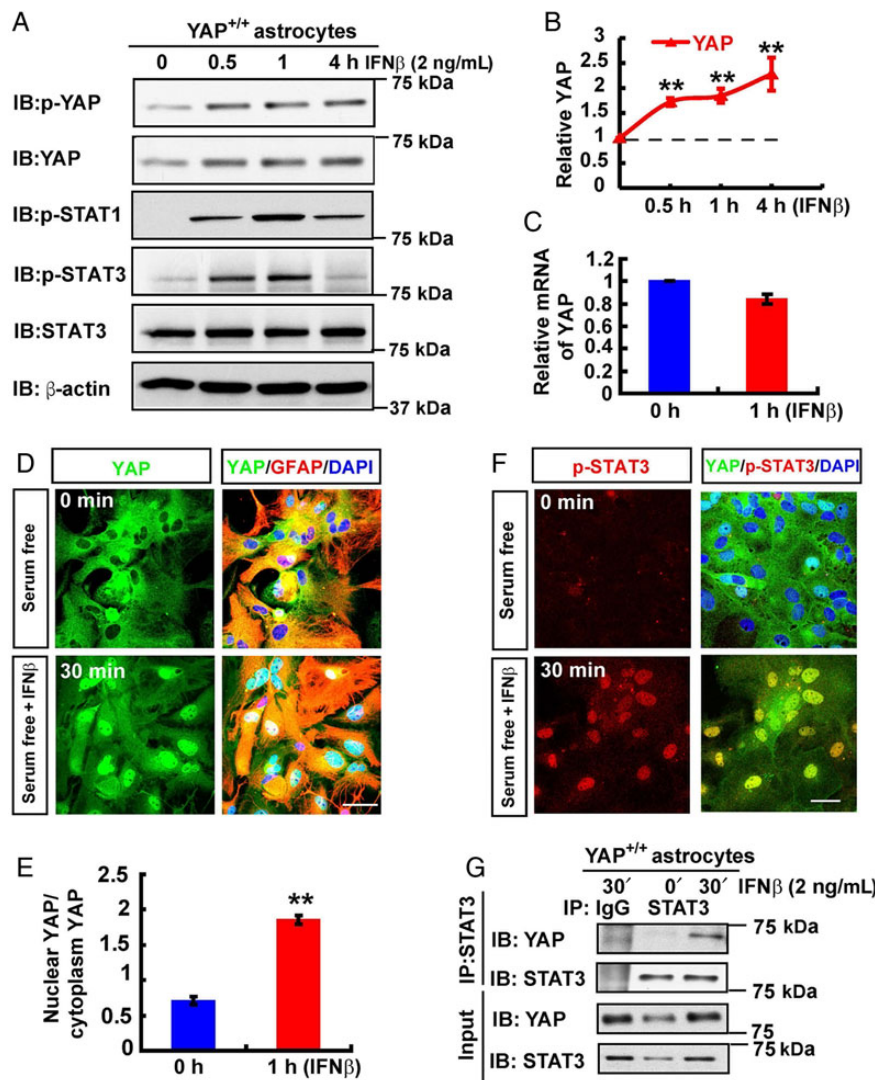
Figure 5. YAP was activated and interacted with STAT3 induced by IFNβ. (A) Astrocytes were serum-starved (serum free DMEM medium) for one overnight (~12 h) before the IFNβ stimulation. Western blot detected the downstream signaling of IFNβ in WT astrocytes before and after IFNβ treatment (2 ng/mL) at indicated time point. (B) Quantitative analysis of relative YAP as shown in (A) (n = 3 per group, normalized to 0 h). (C) RT-PCR analysis showed the relative mRNA level of YAP in WT astrocytes before and after IFNβ treatment (2 ng/mL). (D) Double immunostaining analysis of YAP (green) and GFAP (red) in WT astrocytes before and after IFNβ treatment (2 ng/mL). (E) Quantitative analysis of the ratios of nuclear YAP/cytoplasm YAP in astrocytes before and after IFNβ treatment as shown in (D). (F) Double immunostaining analysis of p-STAT3 (red) and YAP (green) in WT astrocytes before and after IFNβ treatment (2 ng/mL). (G) Western blot showed nuclear protein Co-IP results by nuclear complex Co-IP assays in WT astrocytes before and after IFNβ treatment (2 ng/mL). Scale bars, 20 μm. Data were mean ± SEM. **$P < 0.01$, compared with the control group, Student's t-test.

promoted YAP nuclear translocation and increased YAP protein level (Supplementary Fig. 4A,C,E) in WT cells. YAP in astrocytes was also required for CNTF-induced SOCS3 expression (Supplementary Fig. 4A,D). Taken together, these results suggest that YAP is necessary for the SOCS1/3 induction, but not for other cytokines (e.g., CCL3, CCL4, and CCL8), in response to IFNβ or CNTF.

Restoration of the Astrocytic Activation Deficit by Expression of SOCS3 in YAP$^{-/-}$ Astrocytes

We next determined whether YAP induction of SOCS3 in astrocytes is a critical mechanism underlying YAP prevention of astrocytic activation. To address this issue, exogenously SOCS3 (Flag-tagged SOCS3) was expressed into YAP$^{-/-}$ astrocytes. As shown in Figure 6F,G, in YAP$^{-/-}$ astrocytes expressing Flag-SOCS3, lower level of nestin (a marker for active astrocytes) was

detected, when compared with the untransfected astrocytes. Additionally, the SOCS3 expression also reduced IFNβ-driven or CNTF-driven nuclear translocation of p-STAT3, which was detected in untransfected astrocytes (Fig. 6H,I and Supplementary Fig. 4F). Taken together, these results suggest that SOCS3 is a critical downstream protein of YAP in the negative control of JAK–STAT inflammatory pathways in astrocytes, thus preventing reactive astrogliosis.

Altered BBB Structure and Function in Yap^{nestin}-CKO Mice

Note that activated astrocytes and microglia were largely associated with the blood vessels in Yap^{nestin}-CKO mice (Fig. 3). We thus speculate that BBB structure and function may be altered by activated astrocytes and microglia in Yap mutant brain. To test this speculation, P20 mice were intravenously injected with
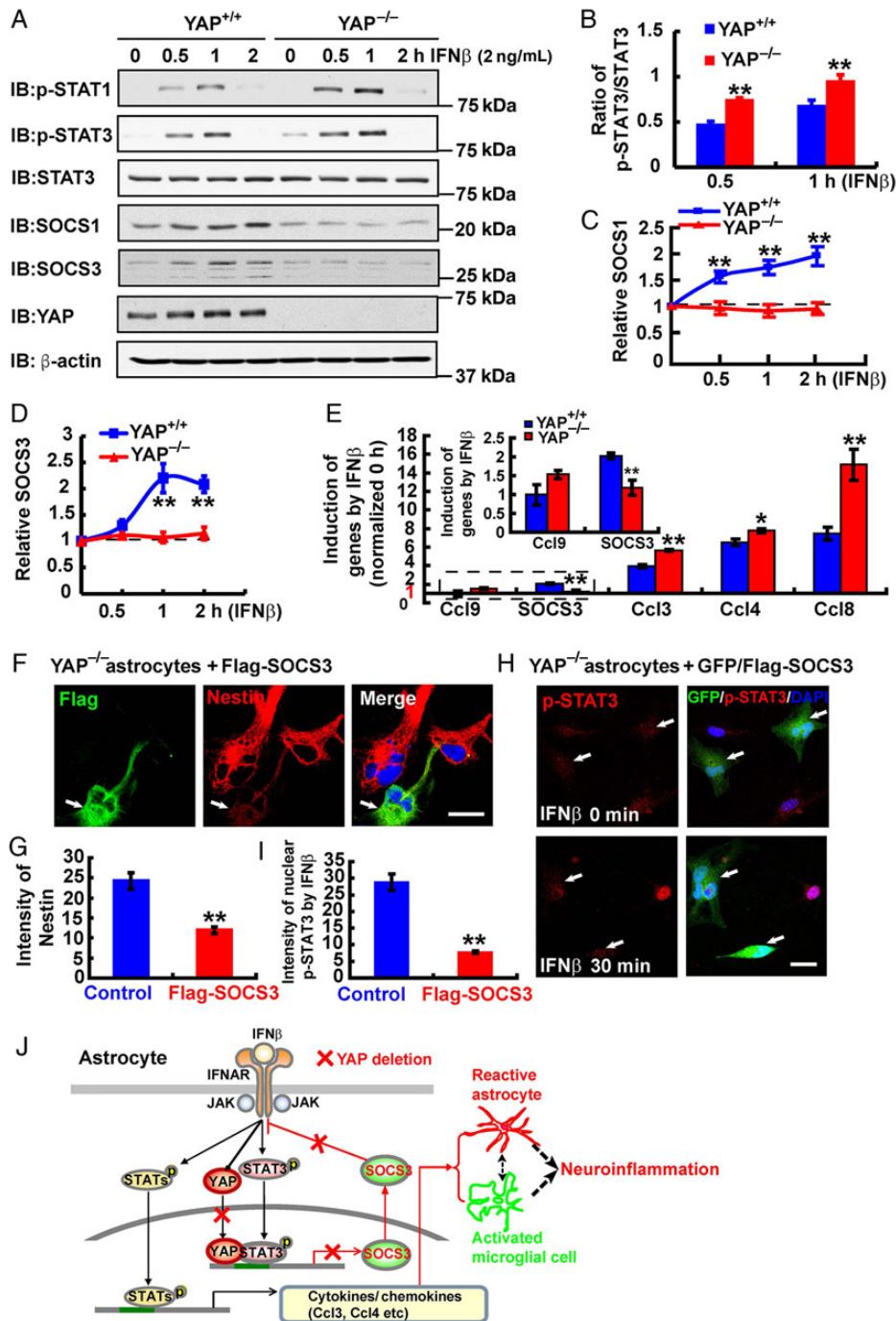
Figure 6. YAP was required for IFNβ-induced SOCS1/3 expression. (A) Astrocytes were serum-starved (0 FBS in the DMEM medium) for one overnight (~12 h) before the IFNβ stimulation. Western blot detected the downstream signaling of IFNβ in WT and YAP⁻/⁻ astrocytes before and after IFNβ treatment (2 ng/mL) at indicated time point. (B–D) Quantitative analysis of the absolute p-STAT3 level (normalized to total STAT3) (B), the relative SOCS1 (C), and SOCS3 (D) (normalized to time zero point) as shown in (A) (n = 3 per group, normalized to 0 h). (E) RT-PCR analysis showed the relative gene expression of Ccl3, Ccl4, Ccl8, Ccl9, and SOCS3 in WT and YAP⁻/⁻ astrocytes before and after IFNβ treatment (2 ng/mL) for 1 h. Selected histogram was shown at higher magnification. (F) Double immunostaining analysis of Flag (green) and nestin (red) in YAP⁻/⁻ astrocytes transfected with Flag-SOCS3. (G) Quantitative analysis of nestin intensity in YAP⁻/⁻ astrocytes transfected with Flag-SOCS3 or untransfected astrocytes. (H) Immunostaining analysis of p-STAT3 (red) in YAP⁻/⁻ astrocytes cotransfected with GFP/Flag-SOCS3 (1 : 3) before and after IFNβ treatment (2 ng/mL). (I) Quantitative analysis of the intensity of nuclear p-STAT3 in YAP⁻/⁻ astrocytes transfected with Flag-SOCS3 induced by IFNβ. (J) A working model illustrates YAP's function in reactive astrocytes and neuroinflammation. White arrowheads indicated transfected astrocytes. Scale bars, 20 μm. Data were mean ± SEM. *P < 0.05, **P < 0.01, compared with the control group, Student's t-test.

exogenous dye tracer (EB), which forms a complex with albumin in blood and is thus unable to pass the BBB (Armulik et al. 2010). Sixteen hours after injection, the dye was obviously accumulated in the brains of the mutant mice, but not in WT mice (Fig. 7A,B), demonstrating impaired BBB permeability in the mutant mice. This view was further confirmed by intravenous injection
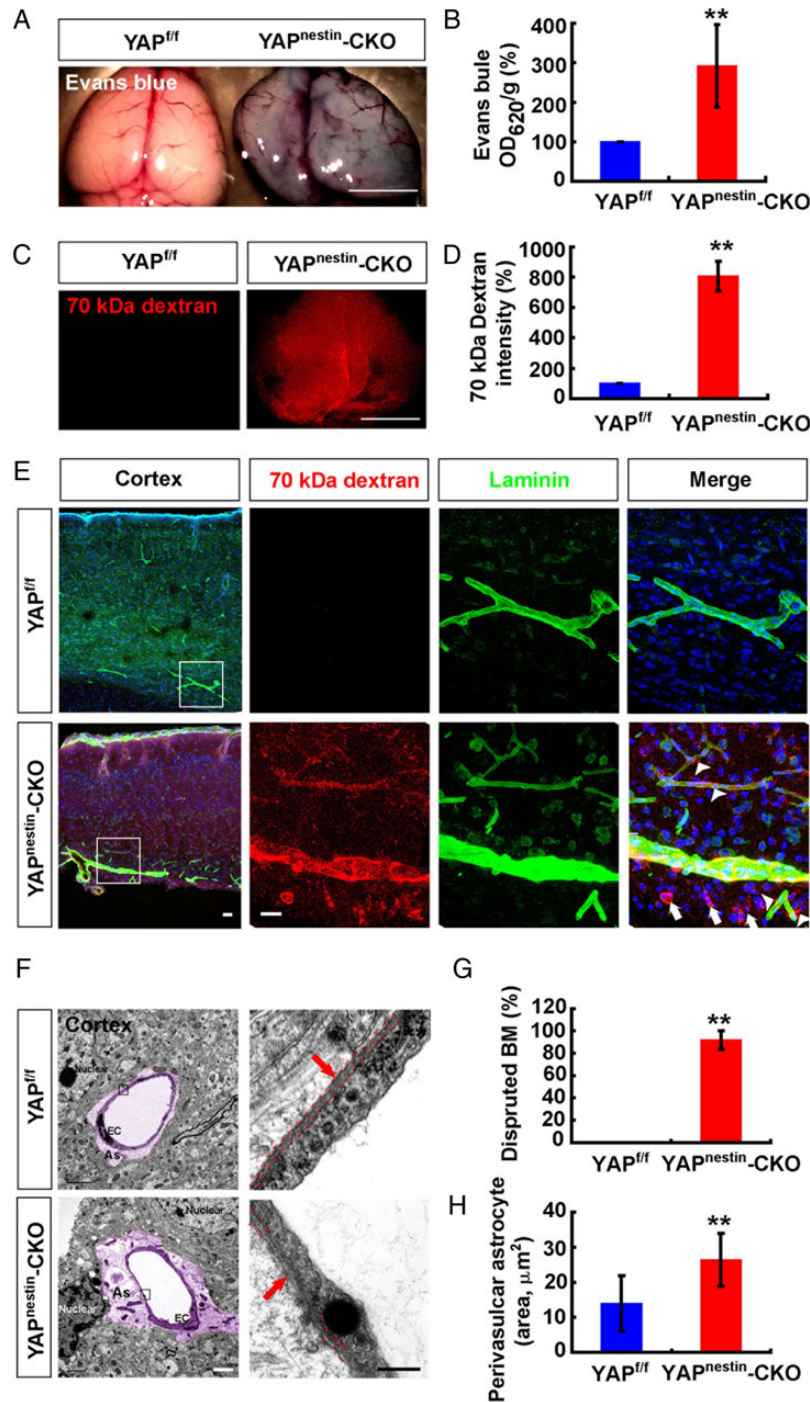
Figure 7. Impaired BBB permeability and altered BBB structure in Yap^{nestin}-CKO brain. (A) Whole brains photographed after EB circulation in P20 Yap$^{f/f}$ and Yap^{nestin}-CKO mice. Scale bar, 5 mm. (B) Quantification of EB dye in P20 Yap$^{f/f}$ and Yap^{nestin}-CKO mice ($n = 3$ per group, normalized to the WT group). (C) Whole brains photographed after 70 kDa dextran circulation in P20 Yap$^{f/f}$ and Yap^{nestin}-CKO mice. Scale bar, 5 mm. (D) Quantification of 70 kDa dextran fluorescence in P20 Yap$^{f/f}$ and Yap^{nestin}-CKO mice ($n = 3$ per group, normalized to the WT group). (E) Confocal images of blood vessels labeled by laminin (green) and 70 kDa dextran (red) in P20 cortex of Yap$^{f/f}$ and Yap^{nestin}-CKO mice (sagittal sections). White arrows indicated the dextran-labeled cells, and white arrowheads indicated the leaked dextran from blood vessels. The selected regions were shown at higher magnification. Scale bars, 20 μm. (F) Electron microscopy images of BBB in P20 cortex of Yap$^{f/f}$ and Yap^{nestin}-CKO mice. Soft pink color indicated BBB unit. As, astrocytes; EC, endothelial cells. Scale bar, 2 μm. The selected regions were shown at higher magnification, Scale bar, 200 nm. Red dotted lines highlight the basal membrane of BBB. (G and H) Quantification of the percentages of disrupted basal membrane ($n = 3$ per group) (G) and perivascular astrocytic end-feet area (H) in Yap$^{f/f}$ and Yap^{nestin}-CKO mice ($n = 10$ for WT group, and $n = 13$ for mutant group). Data were mean ± SD. $^{**}P < 0.01$, compared with the control group, Student's t-test.

of fluorescently labeled 70 kDa dextran, which was also accumulated in the mutant, but not in WT brain (Fig. 7C,D). We next took advantage of the fixable nature of the fluorescent dextran to

explore the route of extravasations in Yap^{nestin}-CKO mice in more detail. The blood vessel was labeled by the antibody against laminin, a key component of basal lamina matrix that surrounds

blood vessels. As shown in Figure 7E, large amounts of 70 kDa dextran fluorescence were detected inside and outside of the blood vessels in Yap[nestin]-CKO cortex, but not in WT, consistent with impaired BBB permeability in YAP mutant mice. Indeed, electron microscopy (EM) analysis showed a thinner, discontinuous basement membrane of BBB in the mutant cortex, compared with WT controls (Fig. 7F,G). Additionally, perivascular astrocytic end-feet was enlarged and swollen in Yap[nestin]-CKO cortex (Fig. 7F,H). These observations demonstrate a broken BBB structure with increased BBB permeability in Yap[nestin]-CKO brain.

Discussion

In this study, we present evidence for YAP's function in suppression of reactive astrogliosis and propose a working model depicted in Figure 6J. In this model, YAP regulates SOCS1/3 expression in astrocytes in response to cytokine stimulation, such as IFNb or CNTF. Thus, YAP deficient astrocytes showed hyper-action of JAK-STAT inflammatory pathway and reactive astrogliosis, which may result in activation of microglia and neuroinflammation, associated with BBB dysfunctions.

How does YAP prevent astrocytic activation? SOCS family proteins are often induced by cytokines and act in a negative-feedback loop to inhibit cytokine signaling transduction (Yoshimura et al. 2007). Here, we provide evidence that IFNβ promotes the nuclear translocation of YAP, where YAP interacted with p-STAT3 to induce SOCS1/3 expression in astrocytes. YAP in astrocytes is required for both IFNβ- and CNTF-induced SOCS3 expression. Deletion of YAP thus results in a hyperactivation of STAT inflammatory pathway in astrocytes, leading to a vicious cycle of neuroinflammation and elevated expression of many cytokines. Expression of SOCS3 in YAP$^{-/-}$ astrocytes prevented the hyperactivation of STAT3 and partially restored the astrocytic activation. Interestingly, in early stage (1 week after injury) of the spinal cord injury mice model, astrocytes are more easily activated in SOCS3 mutant mice, compared with control mice (Okada et al. 2006). These results suggest that YAP induction of SOCS3 is critical for the negative control of JAK–STAT inflammatory pathway and to maintain astrocyte in a resting state.

We noted that in spinal cord injury model, reactive astrocytes in STAT3 conditional knockout mice showed limited migration and resulted in markedly widespread infiltration of inflammatory cells, whereas reactive astrocytes showed rapid migration and secluded inflammatory cells in SOCS3 conditional knockout mice (Okada et al. 2006; Herrmann et al. 2008). Gp130 conditional knockout in astrocytes causes the apoptosis of astrocytes, which increases inflammation (Haroon et al. 2011). In fact, reactive astrocytes can exhibit a vast range of responses as determined by different conditions (Burda and Sofroniew 2014). The reactive astrocytes can produce and release diverse pro- or anti-inflammatory cytokines, chemokines, and neutrophins to cause tissue damage or repair dependent on different pathological insults (Shen et al. 2012; Yang et al. 2012; Burda and Sofroniew 2014; Choi et al. 2014; Xie and Yang 2015). Our in culture and in vivo data showed that reactive astrocytes by YAP deletions caused microglial activation and neuroinflammation. The different observations may result from different pathological conditions (spinal cord injury versus neuroinflammation) or brain regions (spinal cord versus cortex) examined and other target genes regulated by YAP, such as SOCS1 and SOCS2, may be also involved in astrocyte activation.

Abnormal BBB structure or dysfunction of BBB is implicated in multiple neurological disorders (Abbott and Friedman 2012). Astrocytes are an important component of BBB and the abnormal activation of astrocytes may increase expression and secretion of cytokines (e.g., TNF-α, TGFβ1, and IL3) and chemokines (e.g., Ccl3, Ccl4, and Ccl8) that may activate and attract microglia, increase neuroinflammation, and disrupt the endothelial cell–cell junctions and BBB functions (Abbott 2000; da Cruz-Hofling et al. 2009; Argaw et al. 2012; Chapouly et al. 2015; Elahy et al. 2015). Consistent with these previous studies, our findings indicate that it is likely that the abnormal activation of astrocytes by YAP depletion leads to the microglial activation and neuroinflammation, which may result into BBB dysfunction. It is interest to further examine how astrocyte activation by YAP deletion results into BBB dysfunction in future.

In summary, our study not only identifies YAP's unrecognized functions in astrocytic activation, but also reveals a pathway of YAP-SOCS for the negatively control of STAT-mediated inflammatory response.

References

Abbott NJ. 2000. Inflammatory mediators and modulation of blood-brain barrier permeability. Cell Mol Neurobiol. 20: 131–147.

Abbott NJ, Friedman A. 2012. Overview and introduction: the blood-brain barrier in health and disease. Epilepsia. 53 (Suppl 6):1–6.

Abbott NJ, Patabendige AA, Dolman DE, Yusof SR, Begley DJ. 2010. Structure and function of the blood-brain barrier. Neurobiol Dis. 37:13–25.

Argaw AT, Asp L, Zhang J, Navrazhina K, Pham T, Mariani JN, Mahase S, Dutta DJ, Seto J, Kramer EG, et al. 2012. Astrocyte-derived VEGF-A drives blood-brain barrier disruption in CNS inflammatory disease. J Clin Invest. 122:2454–2468.

Armulik A, Genove G, Mae M, Nisancioglu MH, Wallgard E, Niaudet C, He L, Norlin J, Lindblom P, Strittmatter K, et al. 2010. Pericytes regulate the blood-brain barrier. Nature. 468:557–561.

Burda JE, Sofroniew MV. 2014. Reactive gliosis and the multicellular response to CNS damage and disease. Neuron. 81:229–248.

Chapouly C, Tadesse Argaw A, Horng S, Castro K, Zhang J, Asp L, Loo H, Laitman BM, Mariani JN, Straus Farber R, et al. 2015. Astrocytic TYMP and VEGFA drive blood-brain barrier opening

in inflammatory central nervous system lesions. Brain. 138:1548–1567.

Choi SS, Lee HJ, Lim I, Satoh J, Kim SU. 2014. Human astrocytes: secretome profiles of cytokines and chemokines. PLoS ONE. 9:e92325.

da Cruz-Hofling MA, Raposo C, Verinaud L, Zago GM. 2009. Neuroinflammation and astrocytic reaction in the course of *Phoneutria nigriventer* (armed-spider) blood-brain barrier (BBB) opening. Neurotoxicology. 30:636–646.

Elahy M, Jackaman C, Mamo JC, Lam V, Dhaliwal SS, Giles C, Nelson D, Takechi R. 2015. Blood-brain barrier dysfunction developed during normal aging is associated with inflammation and loss of tight junctions but not with leukocyte recruitment. Immun Ageing 12:2.

Eroglu C, Barres BA. 2010. Regulation of synaptic connectivity by glia. Nature. 468:223–231.

Farina C, Aloisi F, Meinl E. 2007. Astrocytes are active players in cerebral innate immunity. Trends Immunol. 28:138–145.

Ge WP, Miyawaki A, Gage FH, Jan YN, Jan LY. 2012. Local generation of glia is a major astrocyte source in postnatal cortex. Nature. 484:376–380.

Guo F, Ma J, McCauley E, Bannerman P, Pleasure D. 2009. Early postnatal proteolipid promoter-expressing progenitors produce multilineage cells in vivo. J Neurosci. 29:7256–7270.

Haroon F, Drogemuller K, Handel U, Brunn A, Reinhold D, Nishanth G, Mueller W, Trautwein C, Ernst M, Deckert M, et al. 2011. Gp130-dependent astrocytic survival is critical for the control of autoimmune central nervous system inflammation. J Immunol. 186:6521–6531.

Herrmann JE, Imura T, Song B, Qi J, Ao Y, Nguyen TK, Korsak RA, Takeda K, Akira S, Sofroniew MV. 2008. STAT3 is a critical regulator of astrogliosis and scar formation after spinal cord injury. J Neurosci. 28:7231–7243.

Liebner S, Czupalla CJ, Wolburg H. 2011. Current concepts of blood-brain barrier development. Int J Dev Biol. 55:467–476.

Mo JS, Park HW, Guan KL. 2014. The Hippo signaling pathway in stem cell biology and cancer. EMBO Rep. 15:642–656.

Moyse E, Segura S, Liard O, Mahaut S, Mechawar N. 2008. Microenvironmental determinants of adult neural stem cell proliferation and lineage commitment in the healthy and injured central nervous system. Curr Stem Cell Res Ther. 3:163–184.

Okada S, Nakamura M, Katoh H, Miyao T, Shimazaki T, Ishii K, Yamane J, Yoshimura A, Iwamoto Y, Toyama Y, et al. 2006. Conditional ablation of Stat3 or Socs3 discloses a dual role for reactive astrocytes after spinal cord injury. Nat Med. 12:829–834.

Pan D. 2010. The hippo signaling pathway in development and cancer. Dev Cell. 19:491–505.

Pekny M, Wilhelmsson U, Pekna M. 2014. The dual role of astrocyte activation and reactive gliosis. Neurosci Lett. 565:30–38.

Piccolo S, Dupont S, Cordenonsi M. 2014. The biology of YAP/TAZ: Hippo signaling and beyond. Physiol Rev. 94:1287–1312.

Qin H, Niyongere SA, Lee SJ, Baker BJ, Benveniste EN. 2008. Expression and functional significance of SOCS-1 and SOCS-3 in astrocytes. J Immunol. 181:3167–3176.

Ransohoff RM, Engelhardt B. 2012. The anatomical and cellular basis of immune surveillance in the central nervous system. Nat Rev Immunol. 12:623–635.

Shen Y, Sun A, Wang Y, Cha D, Wang H, Wang F, Feng L, Fang S. 2012. Upregulation of mesencephalic astrocyte-derived neurotrophic factor in glial cells is associated with ischemia-induced glial activation. J Neuroinflammation. 9:254.

Sofroniew MV, Vinters HV. 2010. Astrocytes: biology and pathology. Acta Neuropathol. 119:7–35.

Su Z, Yuan Y, Chen J, Cao L, Zhu Y, Gao L, Qiu Y, He C. 2009. Reactive astrocytes in glial scar attract olfactory ensheathing cells migration by secreted TNF-alpha in spinal cord lesion of rat. PLoS ONE. 4:e8141.

Tajes M, Ramos-Fernandez E, Weng-Jiang X, Bosch-Morato M, Guivernau B, Eraso-Pichot A, Salvador B, Fernandez-Busquets X, Roquer J, Munoz FJ. 2014. The blood-brain barrier: structure, function and therapeutic approaches to cross it. Mol Membr Biol. 31:152–167.

Takano T, Tian GF, Peng W, Lou N, Libionka W, Han X, Nedergaard M. 2006. Astrocyte-mediated control of cerebral blood flow. Nat Neurosci. 9:260–267.

Taniguchi K, Wu LW, Grivennikov SI, de Jong PR, Lian I, Yu FX, Wang K, Ho SB, Boland BS, Chang JT, et al. 2015. A gp130-Src-YAP module links inflammation to epithelial regeneration. Nature. 519:57–62.

Wang J, Yu RK. 2013. Interaction of ganglioside GD3 with an EGF receptor sustains the self-renewal ability of mouse neural stem cells in vitro. Proc Natl Acad Sci USA. 110:19137–19142.

Wang Y, Hu G, Liu F, Wang X, Wu M, Schwarz JJ, Zhou J. 2014. Deletion of yes-associated protein (YAP) specifically in cardiac and vascular smooth muscle cells reveals a crucial role for YAP in mouse cardiovascular development. Circ Res. 114:957–965.

Xie L, Yang SH. 2015. Interaction of astrocytes and T cells in physiological and pathological conditions. Brain Res. 1623:63–73.

Yang Q, Feng B, Zhang K, Guo YY, Liu SB, Wu YM, Li XQ, Zhao MG. 2012. Excessive astrocyte-derived neurotrophin-3 contributes to the abnormal neuronal dendritic development in a mouse model of fragile X syndrome. PLoS Genet. 8:e1003172.

Yoshimura A, Naka T, Kubo M. 2007. SOCS proteins, cytokine signalling and immune regulation. Nat Rev Immunol. 7:454–465.

Zhang N, Bai H, David KK, Dong J, Zheng Y, Cai J, Giovannini M, Liu P, Anders RA, Pan D. 2010. The Merlin/NF2 tumor suppressor functions through the YAP oncoprotein to regulate tissue homeostasis in mammals. Dev Cell. 19:27–38.

Zhao B, Wei X, Li W, Udan RS, Yang Q, Kim J, Xie J, Ikenoue T, Yu J, Li L, et al. 2007. Inactivation of YAP oncoprotein by the Hippo pathway is involved in cell contact inhibition and tissue growth control. Genes Dev. 21:2747–2761.